Effect of 2-(4-fluorophenylamino)-5-(2,4-dihydroxyphenyl)-1,3,4-thiadiazole on the molecular organisation and structural properties of the DPPC lipid multibilayers

ARTICLE *in* BIOCHIMICA ET BIOPHYSICA ACTA · JULY 2012

Impact Factor: 4.66 · DOI: 10.1016/j.bbamem.2012.07.013 · Source: PubMed

7 AUTHORS, INCLUDING:

Daniel M Kamiński
University of Life Sciences in Lublin
48 PUBLICATIONS **328** CITATIONS
SEE PROFILE

Arkadiusz Matwijczuk
University of Life Sciences in Lublin
26 PUBLICATIONS **45** CITATIONS
SEE PROFILE

Mirosława Dmowska
Maria Curie-Sklodowska University in Lublin
8 PUBLICATIONS **25** CITATIONS
SEE PROFILE

Mariusz Gagoś
Agricultural University in Lublin
52 PUBLICATIONS **443** CITATIONS
SEE PROFILE

(This is a sample cover image for this issue. The actual cover is not yet available at this time.)

Biochimica et Biophysica Acta 1818 (2012) 2850–2859

Contents lists available at SciVerse ScienceDirect

Biochimica et Biophysica Acta

journal homepage: www.elsevier.com/locate/bbamem

Effect of 2-(4-fluorophenylamino)-5-(2,4-dihydroxyphenyl)-1,3,4-thiadiazole on the molecular organisation and structural properties of the DPPC lipid multibilayers

Daniel M. Kamiński [a,c], Arkadiusz Matwijczuk [b], Damian Pociecha [c], Ewa Górecka [c], Andrzej Niewiadomy [a], Mirosława Dmowska [d], Mariusz Gagoś [b,d,*]

[a] Department of Chemistry, University of Life Sciences in Lublin, Akademicka 15, 20-950 Lublin, Poland
[b] Department of Biophysics, University of Life Sciences in Lublin, Akademicka 13, 20-950 Lublin, Poland
[c] Department of Chemistry, Warsaw University 02-093 Warszawa, Pasteura 1, Poland
[d] Department of Cell Biology, Institute of Biology and Biotechnology, Maria Curie-Skłodowska University, 20-033 Lublin, Poland

ARTICLE INFO

Article history:
Received 29 March 2012
Received in revised form 17 July 2012
Accepted 18 July 2012
Available online 24 July 2012

Keywords:
1,3,4-Thiadiazole
DPPC lipid
Multibilayer
X-ray diffraction
FTIR spectroscopy

ABSTRACT

Interactions and complex formation between lipids and biologically active compounds are crucial for better understanding of molecular mechanisms occurring in living cells. In this paper a molecular organisation and complex formation of 2-(4-fluorophenylamino)-5-(2,4-dihydroxybenzeno)-1,3,4-thiadiazole (FABT) in DPPC multibilayers are reported. The simplified pseudo binary phase diagram of this system was created based on the X-ray diffraction study and fourier transform infrared spectroscopic data. The detailed analysis of the refraction effect indicates a much higher concentration of FABT in the polar zones during phase transition. Both the lipid and the complex ripple after cooling. It was found that FABT occupied not only the hydrophilic zones of the lipid membranes but also partly occupied the central part of the non polar zone. The infrared spectroscopy study reveals that FABT strongly interact with hydrophilic (especially PO_2^-) and hydrophobic (especially "kink" vibrations of CH_2 group). The interactions of FABT molecules with these groups are responsible for changes of lipid multibilayers observed in X-ray diffraction study.

1. Introduction

The most important clinical problem related to the use of new therapeutic strategies is the high toxicity of new, potentially cytotoxic compounds. This is caused by the lack of clear biochemical differences between tumour and normal cells and non-specificity of the antitumour action of cytostatics [1,2].

High expectations for therapies are attached to the extensive ongoing research conducted on the group of 2-amino-1,3,4-thiadiazole substituted with 2,4-dihydroxyphenyl group [3–6]. The literature presents the variously-substituted 1,3,4-thiadiazoles as compounds with a broad spectrum of biological activity [7–9]. 2-(4-fluorophenylamino)-5-(2,4-dihydroxyphenyl)-1,3,4-thiadiazole, hereafter abbreviated (FABT), belongs to a large family of 2,4-dihydroxyphenylo-1,3,4-thiadiazoles which exhibit antiproliferative activity in vitro against human tumour cell lines: bladder cancer HCV29T, lung A549, colorectal SW707 and breast cancer T47D [3,10,11]. FABT has also fungistatic properties [5]. FABT molecules exhibit keto-enol tautomery with a significant equilibrium shift towards keto form in n-alkane solvents [12]. The structure of this compound was first time confirmed by structural crystallography [13] where FABT was crystallised in the ionic form.

It is believed that the FABT biological activity has to be partly related to its interactions with lipid membranes. It has been found that FABT does not only change the lipid layers dynamics and stiffness but can also form complexes with lipids similar to: benzothiazoles [14], α-tocopherol [15], dipalmitoylglycerol [16], polymers [17] and DNA [18]. Investigations of interactions between aminothiadiazoles with biological membranes as well as an analysis of the dynamics of these interactions may prove crucial for understanding these mechanisms.

The combination of X-ray diffraction and FTIR spectroscopy techniques facilitates the study of molecular organisation, multilayer dynamics, and lipid-FABT interactions in the lipid environment.

2. Materials and methods

The structure and crystallisation of 2-(4-fluorophenylamino)-5-(2,4-dihydroxybenzeno)-1,3,4-thiadiazole (**FABT**) are described by Kaminski at al. [13] and the synthesis of FABT and its derivatives can be found in the references [19,20]. The schematic structure is presented in Scheme 1. The purity of the compound was 99%. The purity of the lipid dipalmitoylphosphatidylcholine (DPPC) was 99%; therefore, it was used without further purification. All the solvents used were purchased from Sigma Chem. Co. (USA).

* Corresponding author at: Department of Biophysics, University of Life Sciences in Lublin 20-950 Lublin, Poland. Tel.: +48 81 4456899; fax: +48 81 4456684.
E-mail address: mariusz.gagos@up.lublin.pl (M. Gagoś).

0005-2736/$ – see front matter © 2012 Elsevier B.V. All rights reserved.
doi:10.1016/j.bbamem.2012.07.013

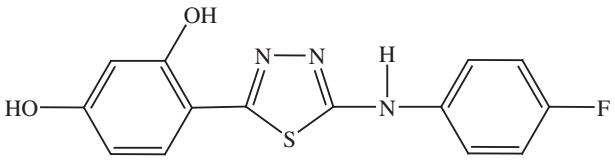

Scheme 1. FABT molecule.

3. Multilayer preparation

The sample preparation procedure is very similar to the one described in references [14,21]. First, the lipids were dissolved in chloroform at a concentration of 1×10^{-2} M. The FABT was dissolved in methanol at a concentration of 5×10^{-3} M. Both solutions were mixed in a 2 mL vial and the solvents were evaporated under a N_2 stream and then under vacuum for ~2 h. After complete solvent evaporation, 0.5 mL of ultrapure water was added and the mixture was homogenised with a sonicator (Bandelin Sonoplus) 3× for 1 s with 60% of total power. Finally, the mixture was deposited on mica plates. Afterwards, the samples were left for 24 h at 24 °C in N_2 atmosphere until complete water evaporation. The multibilayers thus prepared were subjected to the X-ray investigation. In the case of FTIR technique, the water mixture was deposited on the Ge attenuated total reflectance (ATR) crystal.

4. X-ray measurements

X-ray diffraction patterns were collected with a Bruker D8 Discover system, working in the reflection mode. A parallel beam of CuKα radiation (line focus) was formed by Gebel mirror, and the diffracted intensity was controlled with a scintillation counter. Sample temperature was stabilised by the Anton Parr DCS350 heating stage (with accuracy 0.1 °C). Precision sample positioning was assured by the Eulerian cradle mounted on the goniometer.

After alignment the samples were heated from 25 °C to 70 °C and then cooled to 25 °C with temperature step of 1 °C. The X-ray patterns were recorded after temperature stabilisation. The relative humidity of air in experimental hutch was around 30%.

5. FTIR measurements

Infrared absorption spectra were recorded with a 670-IR Varian spectrometer. The attenuated total reflection (ATR) configuration was used with 10 internal reflections of the ATR Ge crystal plate (45° cut). Typically, 25 scans were collected, Fourier-transformed and averaged for each measurement. Absorption spectra at a resolution of one data point per 1 cm^{-1} were obtained in the region between 4000 and 600 cm^{-1}. The instrument was continuously purged with N_2 for 40 min. before and during measurements. The Ge crystal plate was cleaned with ultra pure organic solvents from Sigma-Aldrich. The spectral analysis was performed with Grams/AI software from ThermoGalactic Industries (USA).

6. Modelling of multibilayers

The reflection intensity was corrected by standard factors (Lorenz, polarisation and active area) [22]. The peak positions were corrected for the refraction effect according to Eq. (1) presented in a previous paper [23] because a small deviation from Bragg law were observed for small angles.

$$N\lambda = 2d\sqrt{\sin^2\theta - 2\bar{\delta}}, \tag{1}$$

where:

$$\bar{\delta} = x\delta_1 + (1-x)\delta_2 + \frac{1}{2}x(1-x)\left(\sqrt{sin^2\theta-2\delta_1}-\sqrt{sin^2\theta-2\delta_2}\right)^2,$$

N order of reflection, λ wave length, θ angle of incident X-ray beam, d interlayer spacing, $x = d_1/d$ where d_1 is the thickness of a lipid layer with the refraction index n_1 (see bottom part of Fig. 6), $\delta_1 = 1-n_1$ and $\delta_2 = 1-n_2$. In this case, the following parameters were fixed: $d_1 = 20$ Å and $n_1 = 0.999999$. The following parameters related to refraction were fitted: the refraction index n_2 and interlayer spacing d. Because refraction depends in this case on the ratio between refraction indices n_1 and n_2, the n_1/n_2 ratio is presented. The refraction indices change at the level of 1×10^{-6}, which is expected in the case of soft matter for X-ray diffraction.

The diffractometer alignment can have an effect on refraction correction but in this case clear effects from sample are observed. The refraction correction was not very important for pure lipids; thus it was reduced to the simple form of Bragg equation. In the present paper, the momentum transfer vector $\vec{q}$ is related to the interlayer spacing $\vec{d}$ by the equation:

$$\vec{q} = \frac{2\pi}{\vec{d}}.$$

The lipid electron density model is built of four Gauss functions:

$$\rho_{layer}(z) = \sum_{i=1}^{4} A_i e^{-\left(\frac{z-d_i}{<u^2>}\right)^2} \frac{1}{\sqrt{2\pi<u^2>}},$$

with an amplitude of A_i and positions of d_i: 0, yd, $1/2d$ and $(1-y)d$ in a one-dimensional unit cell. In this case, y describes the position of Gauss maximum in fractional coordinates in the lipid 1D unit cell and can have values in the range from 0 to 0.5.

Here, the $<u^2>$ is the average square displacement parameter of the group of atoms described by Gauss functions and was fixed at 3.8 $Å^2$, which is slightly higher than the value suggested by the authors in the reference [24].The Gauss function amplitudes were fitted to obtain the best fit to the data using the χ^2 method. Despite its simplicity, such a model describes the data well and gives consistent results to the other one from literature [25,26]. The total electron density profile is obtained by summation of 70 monolayers in the z direction.

The diffraction intensity profile of the model is obtained after Fourier transform of the periodic electron density profile calculated previously.

$$I(q) = I_e\left|\int_1^{Nd}\rho(z)e^{z\alpha}e^{iqz}dz\right|^2,$$

The $e^{z\alpha}$ coefficient represents X-ray absorption by lipid layers. This correction limits layer interference, thus the diffraction profile is smooth. The α factor is set to 0.001.

The structures which appeared in the system were described by different electron density profiles and the calculated previously intensities I for each structure were added non-coherently $I_{tot} = I_1 + I_2$.

7. Results and discussion

Fig. 1 shows X-ray scans of DPPC with addition of FABT at different temperatures. Comparison of the observed reflections around $2\theta \cong 2°$ with those from bulk crystals of FABT reveals that they come from the new periodic structures of FABT incorporated into the DPPC multibilayers (DPPC–FABT). The reflections originating from DPPC–FABT are marked with C_G and C_L in the figures. The intensities of the new reflection strongly depend on the FABT content. Reflections from the lamellar structure of the complex in the gel and liquid-crystalline phase are most clearly seen at a concentration of 10 mol% FABT (see Fig. 1 reflections C_G and C_L). For the 20 mol% FABT mixture, only the first order reflection from the complex is intense, whereas the other higher order reflections are broad. This is probably related to the

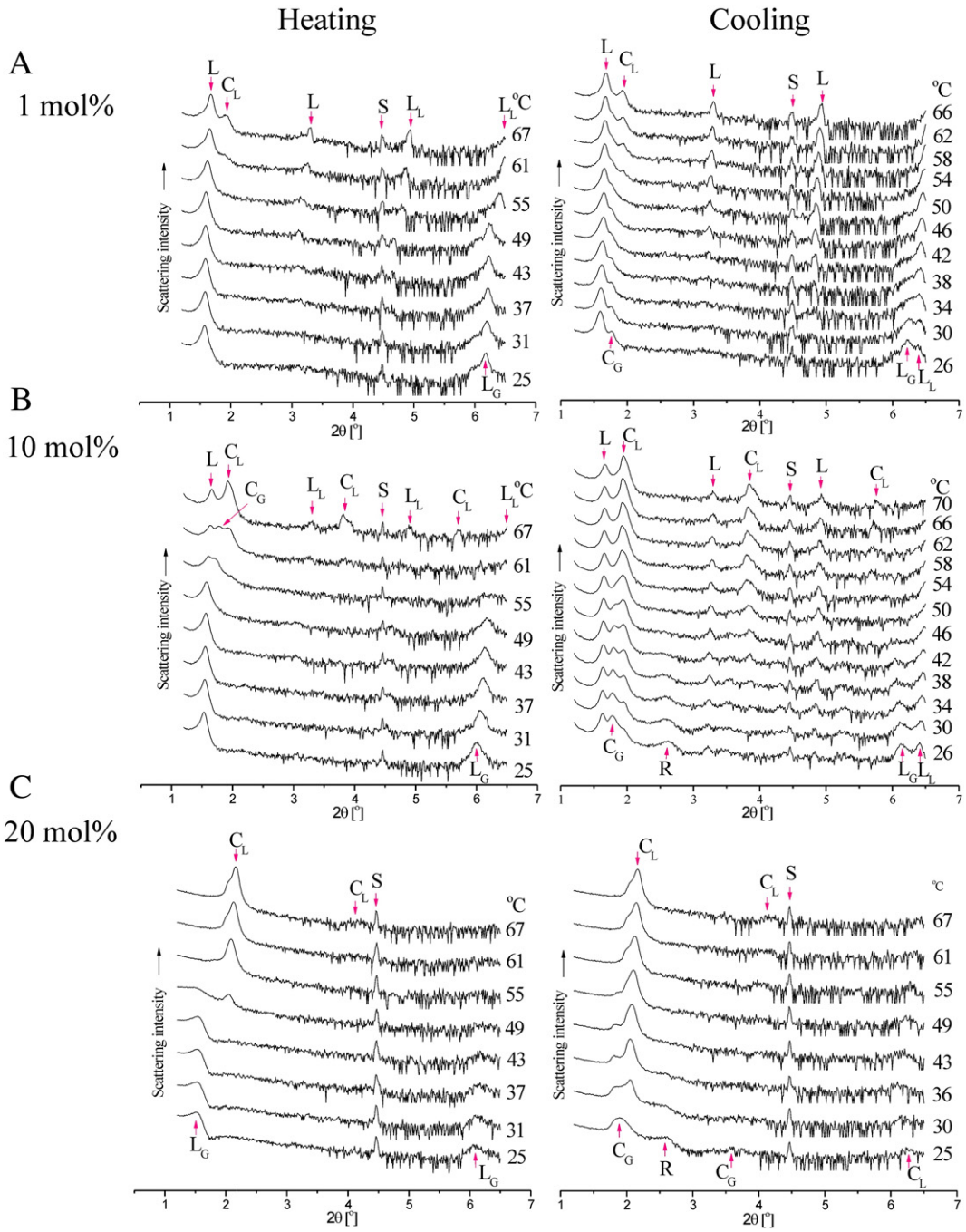

Fig. 1. Selected X-ray diffraction profiles obtained from aqueous dispersion of (A) 1 mol% FABT in DPPC, (B) 10 mol% FABT in DPPC and (C) 20 mol% FABT in DPPC recorded at different temperatures after drying. The symbols denote: L_L — reflections from the lipid multibilayers in the liquid–crystalline phase, L_G — reflections from the lipid multibilayers in the gel phase, C_L — reflections from the lipid–FABT complex in the liquid-crystalline phase, C_G — reflections from the lipid–FABT complex in the gel phase, R — reflection from ripple phase of lipid multibilayers and/or FABT–lipid multibilayers and S — the reflection from mica substrate. In the case where it is impossible to distinguish reflection from lipid in the gel and liquid crystal phase, the L notation is used.

smaller size of the complex domains and complex layer disordered by an excess amount of free FABT. Similar complex formation was recorded in the case of amphotericin B [27], the characteristic reflection related to the complex at the 2θ of ~2° was observed but not described. In all cases, the lamellar repeat structure of the lipid and complex is more pronounced at higher temperatures. This is particularly evident after gel to liquid-crystalline phase transition. To avoid confusion with pure lipid phases, new notations for lipid liquid-crystalline phase and lipid gel phase containing FABT are introduced. Hereafter, lipid in a gel phase (with incorporated FABT) is abbreviated by L_G and lipid in a liquid-crystalline phase (with dissolved FABT) L_L.

The fluorescence microscopy reveals precipitations in the lipid matrix after sample heating. This indicates the L_G and the C_G phase separation at room temperature. The Raman spectroscopy from precipitations (spectra not shown) confirms a higher concentration of FABT in comparison to the rest of the sample (lipid matrix). The areas of the bright zones (DPPC containing FABT) increase with the FABT concentration (see Fig. 2).

Fig. 3 presents temperature dependence of the layer thickness and the ratio of n_1/n_2 refraction indices with temperature for pure DPPC, and the DPPC mixture with 1, 10 and 20 mol% of FABT. The layer thickness of L_G with 1 mol% of FABT is the same as for pure DPPC. At a

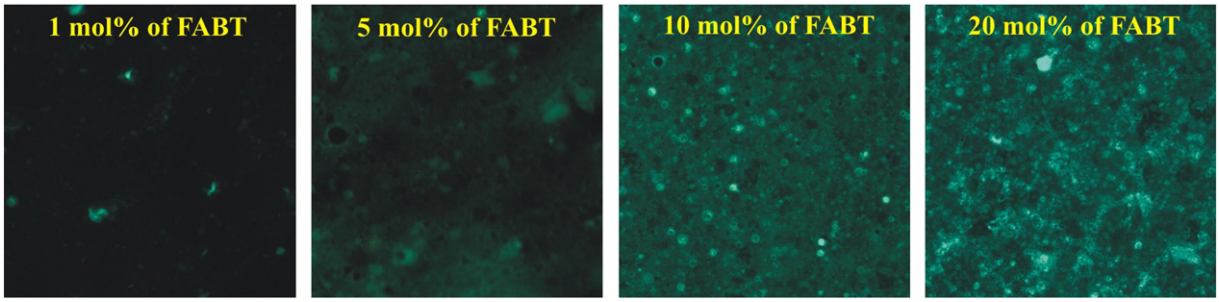

Fig. 2. Dry DPPC multibilayers containing FABT. The pictures were taken with the Leica DM4000 fluorescence microscope. The excitation wavelength was 405 nm. The picture dimensions are 200 μm×200 μm taken with LEICA DM 4000 B microscope.

concentration of 10 mol% FABT, the layer is thicker by about 1 Å than the pure DPPC layer. After the heating-cooling cycle, the lipid layer returns to the thickness similar to the one recorded for pure DPPC. This can be partly related to water evaporation from the multibilayers. This observation can be correlated with FTIR spectra which shows after heating decrease of the band related to −OH vibrations. However, this effect is much weaker by ~0.2 Å (which is in error bar of the measurement) in the case of 1 mol% FABT and thus it should also be correlated (in case of 10 mol% FABT) with FABT surrounding the DPPC layers or FABT rearrangement in the DPPC layers (probably, higher temperature facilitates intermolecular interactions). The L_G layer thickness of 58.2 Å recorded for 20 mol% of FABT is similar to the one observed for 10 mol% of FABT in DPPC. In all the cases, the thickness of lipid layers decreases with temperature but in the case of 10 mol%, the slope exhibits the highest inclination. In all the cases, the L_L phase behaves independently from the complex phase C_L.

Noticeably, the rapid changes in the thickness for 1 mol% and 10 mol% at 52 °C and 57 °C, respectively, are accompanied by refraction changes. The n_1/n_2 ratio for 1 mol% and 10 mol% of FABT in DPPC is the same at the beginning; however, they have different slopes with temperature. Both of them have a higher n_1/n_2 than for pure DPPC, see Fig. 3. For 1 mol% of FABT in DPPC, during heating the gel phase is transformed into the liquid-crystalline one with drastic lowering of the n_1/n_2 ratio. This corresponds to higher electron density in refraction layer 2 compared to layer 1. The ratio returns to the previous value with further heating. A similar effect is observed during cooling. The ratio decreases with cooling and, around 32 °C, there is a jump to the ratio observed for freshly prepared sample. In the case of 10 mol%, the effect is opposite. With temperature, the ratio increases and at 54 °C transition to the liquid-crystalline phase occurs. During cooling, the ratio changes slightly but again at 40 °C transition to the liquid phase with a rapid change in n_1/n_2 occurs. This is related to the higher electron density in refraction layer 1 and lower electron density in refraction layer 2. In both cases, the phase transitions are manifested by deviation from the trend line. These results indicate that for 10 mol% of FABT in a sample this compound moves into the hydrophilic zones of lipid at phase transition but once the new phase is formed the distribution between high and low electron density layers (with refraction indices n_1 and n_2) returns to the previous ratio. For 1 mol% of FABT, the hydrophobic zones of lipid at phase transition have lower electron density because of breaking hydrogen bonds and probably a higher number of defects, which results in higher intermolecular spacing.

The reference X-ray data show that dry DPPC multibilayers have the main transition at much higher temperature [21] than 41.2 °C expected for multibilayers containing water [28,29]. As can be seen, addition of FABT causes a shift of the transition temperature to lower values, in comparison to the pure DPPC, and additionally makes it more smooth (see Fig. 3). For a concentration of 1 mol% FABT, the complete transition of L_G to L_L occurs above ~52 °C, see phase diagram in Fig. 4. However, during cooling the L_L phase occurs already much earlier at ~26 °C (measurement not shown). The precise values of phase transitions can occur at higher temperatures but the values presented are within the detection limit of X-ray data for samples with this FABT concentration. At 10 mol% of FABT, the L_G and C_G phases are completely transformed into L_L and C_L at ~62 °C. The L_L phase disappears at ~38 °C. This can be explained as stiffening of multibilayers caused by FABT, similarly to the one observed in the case of cholesterol [30]. Most probably, FABT molecules are randomly incorporated into DPPC layers (of the L phase), which makes the lipid molecules more rigid. It should be mentioned that at 1 mol% of FABT the reflection from the complex is clearly visible (see Fig. 1); this means that the lipid multibilayer has to be saturated with FABT at much lower molar concentrations of FABT.

8. The complex

For all the concentrations of FABT observed, there is clear immiscibility of DPPC and the complex in the liquid-crystalline and gel phases, which is supported by different sets of reflections, see Fig. 1. However, in all the cases, the lamellar structure of DPPC containing FABT (L_G and L_L and a DPPC–FABT complex) is more pronounced in the case of 1 and 10 mol% FABT in DPPC. The lamellar liquid complex (C_L) has a repeat spacing of 46.0 ± 0.6 Å for 1 and 10 mol% of FABT in DPPC above the gel to liquid phase transition (see Fig 4). In the case of 20 mol% FABT (more pronounced reflections), the interlayer spacing of C_L change into 2.7 Å with temperature, see Fig. 3. However, below the melting temperature, the complex in the gel phase (C_G) has interlayer spacing of 49.9 ± 0.6 Å. Therefore, the complex is transformed into a form with higher interlayer spacing. This behaviour is similar to the one observed in the case of the DPPC complex with dipalmitoylglycerol (DPG) [16]. Interestingly, both phases C_G and C_L coexist together in wide range of temperatures, which is especially clearly seen during the cooling cycle, see Fig. 1. During heating, the transitions are shifted to about 2–4 °C higher. However in static temperature conditions, the range of phase coexistence should probably be much narrower. In all the cases, reflection from complex phase is more pronounced during subsequent cooling scans. First, this can indicate better molecule arrangement in layers and second, larger X-ray scattering domains created most probably on the basis of Ostwald ripening mechanism. During heating, a gel complex reflection C_G appears and simultaneously the intensity of the L reflections decreases. In the cooling cycle, the lipid first-order reflection remains almost constant. This suggests that the periodic complex structure in the gel phase is formed initially during the first heating from the lipid phase and randomly distributed FABT molecules. Subsequent heating or cooling cycles do not change the ratio between lipid containing FABT and the complex.

This hypothesis if fully supported by the observation in the case of 20 mol% FABT in DPPC. The broad reflections from DPPC layer L_G completely disappears and is transformed into the liquid complex C_L at the L_G to L_L transition. This transition point is not accidental because at this temperature lipid multibilayers are the most defected

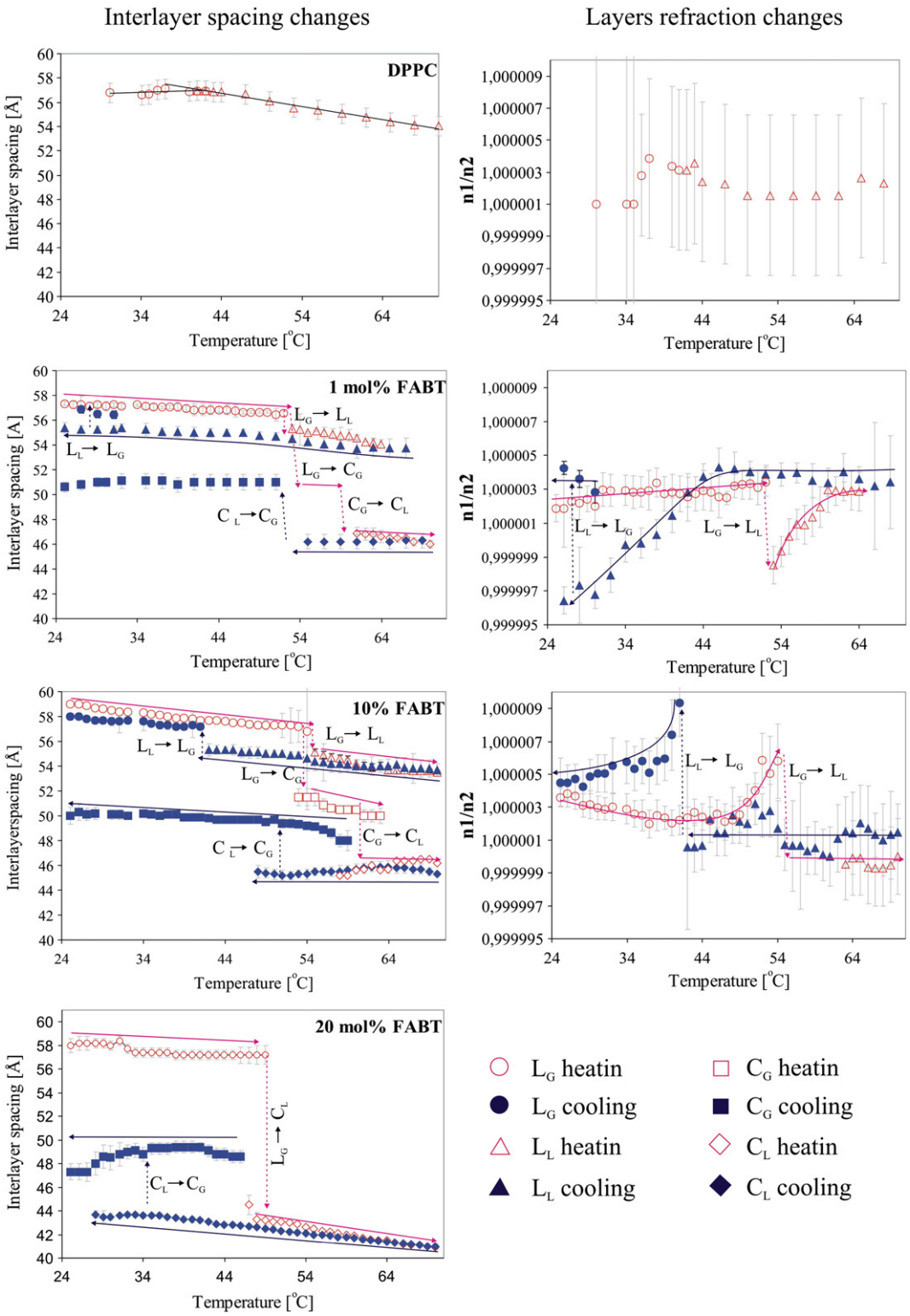

Fig. 3. On the left: interlayer spacing of the DPPC and DPPC–FABT complex at different temperatures. On the right: the ratio of refraction indices n_1/n_2 as a function of temperature for the DPPC multilayer containing FABT. For comparison, data for pure DPPC are presented at the top of this panel. The limited data set in this case leads to much larger error bars. The lines with arrows are for guidance. For 1 mol% of FABT at L_G to C_G transition any experimental points are visible. Most probably this phase exists like for 10 mol% of FABT but the diffraction signal is too weak to be detected.

and FABT molecules can be easily incorporated in the hydrophilic zones of lipid, as indicated by the refraction data. After cooling, the liquid complex is transformed into the C_G phase but reflections from the L_G phase do not appear. This suggests that after first heating close to the lipid phase transition L_G to L_L, the entire DPPC is associated with the FABT forming complex.

9. Complex stoichiometry

Fig. 5 shows integrated peak intensity from L_L and C_L at 70 °C. In the case of the complex, the points are arranged in a straight line. This suggests that the upper limit for the C_L complex is 4:1 (80 mol% DPPC/20 mol% FABT). The different ratio calculated from the peak

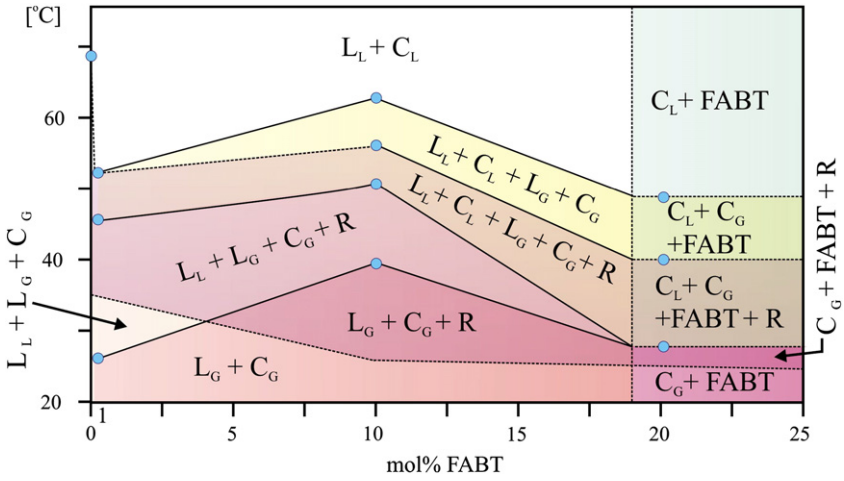

Fig. 4. Simplified pseudo binary phase diagram of DPPC with FABT from heating–cooling measurements (no equilibrium). The blue circles denote measured points during cooling. The phase diagram for heating cycle is around 3–4 °C shifted up. The dashed lines describe approximate positions of phase borders. The complex phase appears at a concentration much lower than 1 mol% of FABT. All abbreviations used are explained in Fig. 1. (For interpretation of the references to colour in this figure legend, the reader is referred to the web version of the article.)

area of L_L can be an effect of disordering of DPPC layers by FABT. This leads to lower X-ray scattered intensities of DPPC peaks, especially at higher concentrations of FABT, which is clearly seen during heating of the 20 mol% FABT mixture (see Fig. 1). This is in agreement with the FTIR study where changes related to the FABT peaks only are observed for 20 mol% of FABT. Taking this into account, the ratio 4:1 should be a lower limit of the complex stoichiometry. Considering only the points at 1 and 10 mol% of FABT, the best integer ratio is 6:1 between DPPC and FABT in the complex. This is the upper limit for the complex stoichiometry.

10. Layer ripples

In the case of 10 mol% FABT in DPPC a broad peak which corresponds to the ripple amplitude of 33.5 Å appears at the temperature range of 57–26 °C during cooling; see Fig. 1 marked by R. The peak has its maximum amplitude at 44 °C. This can be related to the ripple structure of the lipid layers [31,32]. Its amplitude at 26 °C is much smaller than at maximum, which can be related to the smaller tension caused by thermal expansion. The ripping structure does not appear during the first heating of freshly prepared samples. This indicates that first the molecules of FABT have to be incorporated into the L_L layers and then the complex can ripple in a cooling cycle or after heating the layers are less defected and thus more susceptible to ripple. Also, the ripple appears in the case of 20 mol% of FABT where only the complex with free FABT is present in the system. The peak appears between 40 and 25 °C with the observed maximum at 25 °C (the lowest measured temperature). The periodicity corresponds to ~34.6 Å. The ripple peak has a lower amplitude, compared to the sample with 10 mol% FABT. This can be caused by higher stiffening of the complex, compared to the lipid layers and the second, free FABT can suppress the ripple process. Most probably the ripple of the complex and the lipid coexist together but it is impossible, based on the presented diffraction data, to distinguish these two effects, see Fig. 4.

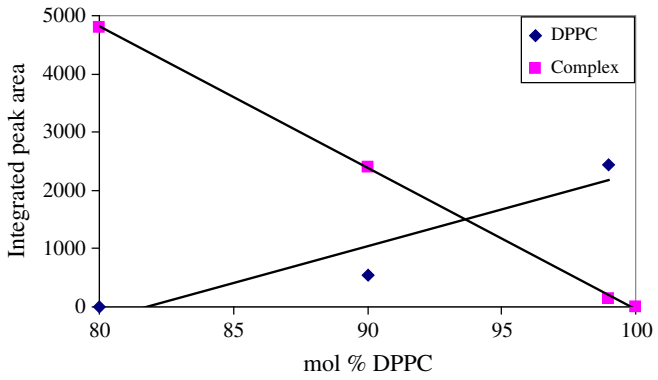

Fig. 5. Integrated intensities of first order peaks of DPPC and FABT in liquid phases at 70 °C. The changes in the peak area of the complex C_L phase are well described by the linear function; however, the integrated area of L_L peaks deviates from the trend line. This can be caused by disordering of L_L layers by free FABT and weaker than expected X-ray scattering from them.

11. Electron density profiles

Fig. 7 presents the electron density profiles obtained after model fitting to the data calculated for DPPC at 30 °C, L_G at 26 °C, L_L at 69 °C and complex C_L at 69 °C. The data for L_L, L_G and C_L are from 10 mol% FABT sample during heating. The diffraction data indicate that FABT incorporated in the DPPC L_G and L_L phases only slightly (left side of the phase diagram, Fig. 4). The electron density profiles of L_G and L_L phases as can be expected remains the one of pure DPPC. A higher concentration of FABT leads to formation of a complex which is mainly seen in the changes in the FTIR spectra. In the case of the complex, FABT concentrates mostly close to the lipid hydrophilic groups, which is visible in much higher electron density profile of the hydrophilic zones of the lipid, see Fig. 7. Also, the electron density profile is higher at the central low electron density part of the lipid bilayer, compared to pure DPPC, which indicates a small amount of FABT incorporated into this layer region. These observations are more precisely discussed in the part concerning the FTIR study. A similar effect of compound cumulating close to the hydrophilic part of the lipid was observed in the case of amphotericin B in DPPC [27].

12. FTIR spectroscopic studies of non-heated samples

To better understand the molecular interaction processes occurring between DPPC and FABT, a FTIR technique was applied. Fig. 7A shows ATR-FTIR normalised spectra of pure DPPC and 5 mol% of FABT in DPPC multibilayers. Fig. 7B shows subtracted spectra of 5 mol% FABT in DPPC minus pure DPPC (subtraction factor f = 1). After incorporation of 1 mol% of FABT into DPPC, clear changes (measured but not shown) are visible in the differential spectrum. FABT interacts with the PO_2^- group, which was observed as spectral changes in the band centred ca. at 1245 cm^{-1} corresponding to PO_2^- antisymmetric vibrations (in the region of 1100–1300 cm^{-1}), see Fig. 8F. For

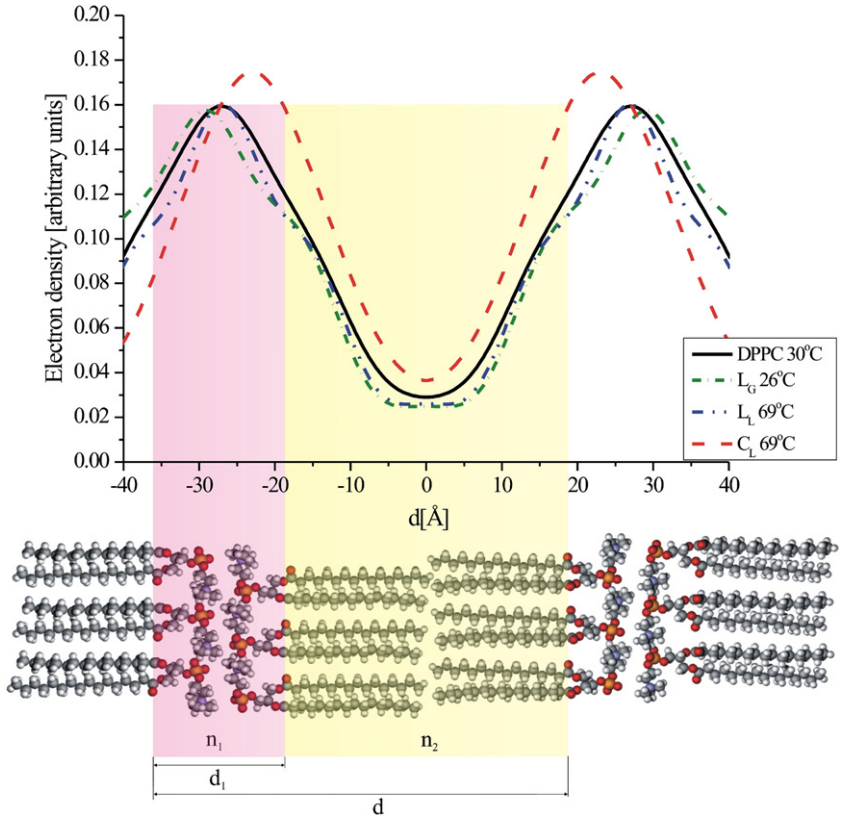

Fig. 6. Electron density profiles of DPPC, DPPC containing FABT (L_G and L_L) and DPPC–FABT complex (C_L) multibilayers.

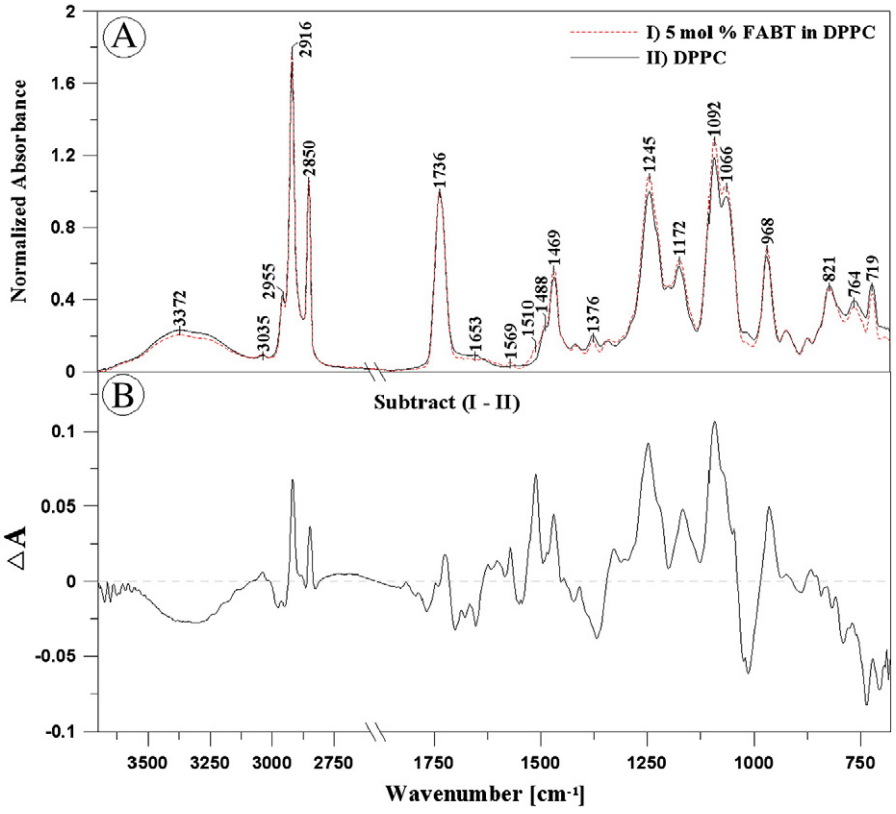

Fig. 7. Infrared absorption spectra of multibilayers formed with pure DPPC lipid and DPPC containing 5 mol% of FABT. The multilayers were deposited on Ge crystal and measured at room temperature.

5 mol% of FABT in DPPC (see, Fig. 7B), more clear changes (an increase in the ΔA) in the discussed region are observed. However, at the concentration of 10 mol% of FABT, the band intensity is decreased and is shifted towards lower frequencies. In the light of the above results, it can be concluded that FABT molecules strongly interact with the PO_2^- group and thus concentrate in the hydrophilic zones of the lipid. In all the spectra presented, a band coming from FABT moieties characteristic for $\delta(N-H)+\nu(C-N)$ vibrations centred at 1510 cm^{-1} is presented [12,14].

Also, changes are observed in the region 1000–1100 cm^{-1}, which is characteristic for skeletal vibrations of C–O–P–O–C in DPPC. At 1 mol% of FABT in DPPC, those changes are not so pronounced but in 5 mol% of FABT in DPPC a very intensive band (centred around 1093 cm^{-1}) is observed in the differential spectrum. However, in 10 mol% and 20 mol%, the changes are not so pronounced as in the sample with 5 mol% of FABT in DPPC. Fig. 8G shows dependence between the FABT concentration and spectral shift of the ν(C–O–P–O–C) band. At the concentrations of 10 and 20 mol% of FABT, the shift occurs towards higher frequencies. The maximum shift towards higher frequencies is observed for 5 mol% of FABT. These results also indicate an interaction between FABT molecules and the hydrophilic zones of the lipid.

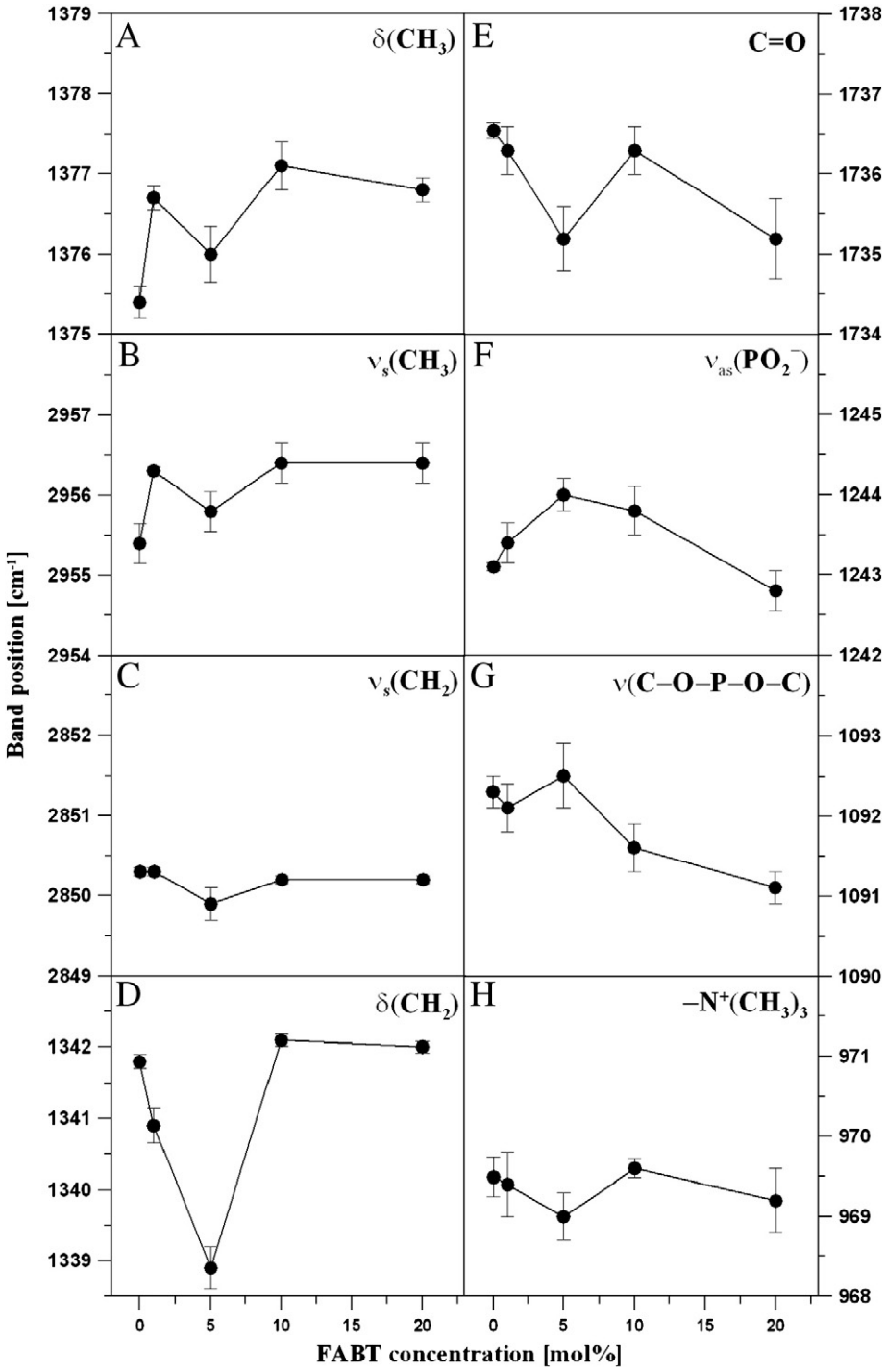

Fig. 8. Dependence of the position of the absorption bands on the FABT molar concentration in the FTIR absorption spectra from DPPC multibilayers (the width of the band position scale in all cases is 4 cm^{-1}).

The changes discussed above are very characteristic for the polar zone of lipids. However, changes in the region 930–1000 cm^{-1} which corresponds to the choline group ($-N^{+}(CH_3)_3$ are not recorded except for 5 mol% of FABT in DPPC, where a shift towards lower frequencies is observed. This can be correlated with the shift to higher frequencies of C–O–P–O–C and PO_2^- groups. This can be explained as an effect of interaction between FABT and the choline group and simultaneous weakening of the hydrogen bonds of C–O–P–O–C between lipids. It should be mentioned that the results described above are for non-heated samples; therefore, the complex formation is not fully completed and free FABT moieties are present in the lipid matrix.

The band centred at 1469 cm^{-1} (see Fig. 7) is characteristic for scissoring deformation vibrations of the methylene ($-CH_2$) group. It changes the intensity but not the spectral shift for all the FABT concentrations measured. Because the band from FABT is also present in the same region, this will not be discussed. Changes in the wagging $-CH_2$ bands between 1300 and 1400 cm^{-1} are observed and can be distinguished from symmetrical deformation vibration of the $-CH_3$ group (called "umbrella") visible in a band centred around 1378 cm^{-1}. Fig. 8A presents the influence of the molar concentration of FABT on the band position. Incorporation of FABT molecules into DPPC increases the frequency, but at 5 mol% a significant shift towards lower frequencies is observed. After that the band shifts again to the frequency recorded for 1 mol% of FABT. These effects are accompanied by changes in the region sensitive for symmetric and asymmetric stretching vibrations of $-CH_2$ and $-CH_3$ groups between 2800 and 3000 cm^{-1} (see Fig. 7). As can be seen in Fig. 8B, a similar effect like that for deformational vibration is observed for the band related to stretching vibrations of the $-CH_3$ group which shifts towards higher frequencies. In contrast, the band related to the stretching $-CH_2$ vibrations remains unchanged for all the concentrations measured. In the light of the above results, it can be concluded that FABT is organised not only close to the polar zone of the lipid but also interacts with methyl groups in the central part of the membrane. Surprisingly, a significant shift is observed in the region between 1338 and 1342 cm^{-1}, characteristic for kink vibrations of $-CH_2$ groups. This suggests that FABT is incorporated in the central part of the membrane and changes conformation of alkane chains. It also has an effect on bilayer thickness.

In the subtracted spectrum in Fig. 7B, changes related to stretching vibrations of the C═O groups are visible. The band from the subtracted spectrum centred at 1724 cm^{-1} shifted towards lower frequencies indicates interactions of FABT molecules with the C═O group through hydrogen bonds. This is in agreement with the X-ray study, where the electron density increased for the polar zone at a low concentration of FABT. At higher concentrations of FABT, a complex, which also has higher electron density in the polar zone, is formed.

13. Conclusions

Incorporation of FABT into DPPC membranes in amounts smaller than 1 mol% leads to changes in the lipid multibilayer molecular organisation. It is observed that the mine phase transition occurs at higher temperature compared to pure DPPC and the transition is smoother. This behaviour is typical for stiffening of the lipid multibilayers. Higher concentrations of FABT lead to formation of the complex with DPPC. The observed complex has a lamellar structure, like the lipid membranes, and occurs in gel and liquid-crystalline phase but the interlayer spacing is smaller. Detailed analysis of refraction indices indicates that during phase transition for 10 mol% of FABT in DPPC, FABT is incorporated into the polar zone of the lipid membrane. After formation of the new phase, the electron density in both zones returns to the initial ratio. Integration of the peak area indicates that the new complex is formed with stoichiometry between 1:4 to 1:6 (FABT:DPPC). The small changes in the liquid-lipid multibilayers induced by heating and cooling can be related to dehydration process. Electron density profiles after data fitting and FTIR spectroscopic data indicate that FABT in the complex is mostly incorporated into the hydrophilic part of the lipid membrane and only in small amounts in the central hydrophobic part. Additionally, it was found that FABT has a strong influence on deformational vibrations of $-CH_2$ and $-CH_3$ vibrations. For stretching vibrations the changes are not so pronounced. These results are very important in biomedical point of view.

References

[1] A.T. Reddy, K. Witek, Neurologic complications of chemotherapy for children with cancer, Curr. Neurol. Neurosci. Rep. 3 (2003) 137–142.
[2] B.A. Chabner, T.G. Roberts Jr., Timeline: chemotherapy and the war on cancer, Nat. Rev. Cancer 5 (2005) 65–72.
[3] J. Matysiak, A. Opolski, Synthesis and antiproliferative activity of N-substituted 2-amino-5-(2,4-dihydroxyphenyl)-1,3,4-thiadiazoles, Bioorg. Med. Chem. 14 (2006) 4483–4489.
[4] J. Matysiak, Z. Malinski, 2-(2,4-Dihydroxyphenyl)-1,3,4-thiadiazole analogues: antifungal activity in vitro against Candida species, Bioorg. Khim. 33 (2007) 640–647.
[5] W. Rzeski, J. Matysiak, M. Kandefer-Szerszen, Anticancer, neuroprotective activities and computational studies of 2-amino-1,3,4-thiadiazole based compound, Bioorg. Med. Chem. 15 (2007) 3201–3207.
[6] J. Matysiak, Evaluation of electronic, lipophilic and membrane affinity effects on antiproliferative activity of 5-substituted-2-(2,4-dihydroxyphenyl)-1,3,4-thiadiazoles against various human cancer cells, Eur. J. Med. Chem. 42 (2007) 940–947.
[7] J.K. Gupta, R. Dudhey, T.K. Sharma, Synthesis and pharmacological activity of substituted 1,3,4-thiadiazole derivatives, Medichemonline 1 (2010) 1001.
[8] N. Siddiqui, P. Ahuja, W. Ahsan, S.N. Pandeya, M.S. Alam, Thiadiazoles: progress report on biological activities, J. Chem. Pharm. Res. 1 (2009) 19–30.
[9] G. Mishra, A.K. Singh, K. Jyoti, Review article on 1,3,4-thiadiazole derivatives and its pharmacological activities, Int. J. Chem. Technol. Res. 3 (2011) 1380–1393.
[10] J. Matysiak, A. Nasulewicz, M. Pelczynska, M. Switalska, I. Jaroszewicz, A. Opolski, Synthesis and antiproliferative activity of some 5-substituted 2-(2,4-dihydroxyphenyl)-1,3,4-thiadiazoles, Eur. J. Med. Chem. 41 (2006) 475–482.
[11] J. Matysiak, Evaluation of antiproliferative effect in vitro of some 2-amino-5-(2,4-dihydroxyphenyl)-1,3,4-thiadiazole derivatives, Chem. Pharm. Bull. (Tokyo) 54 (2006) 988–991.
[12] M. Gagoś, A. Matwijczuk, D. Kaminski, A. Niewiadomy, R. Kowalski, G.P. Karwasz, Spectroscopic studies of intramolecular proton transfer in 2-(4-fluorophenylamino)-5-(2,4-dihydroxybenzeno)-1,3,4-thiadiazole, J. Fluoresc. 21 (2011) 1–10.
[13] D.M. Kaminski, A.A. Hoser, M. Gagoś, A. Matwijczuk, M. Arczewska, A. Niewiadomy, K. Wozniak, Solvatomorphism of 2-(4-Fluorophenylamino)-5-(2,4-dihydroxybenzeno)-1,3,4-thiadiazole chloride, Cryst. Growth Des. 10 (2010) 3480–3488.
[14] M. Gagoś, Molecular organization of 2-(2,4-dihydroxylphenyl)-5,6-dichlor 1,3-benzothiazole in monomolecular layers formed with diphytanoylphosphatidylcholine: a linear dichroism-FTIR study, Biochim. Biophys. Acta 1778 (2008) 2520–2525.
[15] X. Wang, P.J. Quinn, The structure and phase behaviour of alpha-tocopherol-rich domains in 1-palmitoyl-2-oleoyl-phosphatidylethanolamine, Biochimie 88 (2006) 1883–1888.
[16] P.J. Quinn, H. Takahashi, I. Hatta, Characterization of complexes formed in fully hydrated dispersions of dipalmitoyl derivatives of phosphatidylcholine and diacylglycerol, Biophys. J. 68 (1995) 1374–1382.
[17] C. Erdelen, A. Laschewsky, H. Ringsdorf, J. Schneider, A. Schuster, Thermal-behavior of polymeric Langmuir–Blodgett multilayers, Thin Solid Films 180 (1989) 153–166.
[18] I. Koltover, T. Salditt, C.R. Safinya, Phase diagram, stability, and overcharging of lamellar cationic lipid-DNA self-assembled complexes, Biophys. J. 77 (1999) 915–924.
[19] J. Matysiak, A. Niewiadomy, Application of sulfinyl bis(2,4-dihydroxythiobenzoyl) in the synthesis of N-substituted 2-amino-5-(2,4-dihydroxyphenyl)-1,3,4-thiadiazoles, ChemInform 37 (43) (2006) 1621–1630.
[20] A. Niewiadomy, J. Matysiak, The method of synthesis of 2-aryl(alkyl, alkenyl) amino-5-(2,4-dihydroxybenzene)-1,3,4-thiadiazoles, in, Patent pending, P362805, Poland, 2003.
[21] H. Nagase, H. Ueda, I.M. Nakagaki, Temperature change of the lamellar structure of DPPC/disaccharide/water systems with low water content, Biochim. Biophys. Acta Biomembr. 1371 (1998) 223–231.
[22] E. Vlieg, J. Appl. Crystallogr. 30 (1997) 532.
[23] J. Xiaoming, W. Ziqin, Bragg's law with refractive correction of low-angle x-ray diffraction for periodic multilayers, Chin. Phys. Lett. 8 (1991) 356.
[24] D. Jacquemain, S.G. Wolf, F. Leveiller, M. Deutsch, K. Kjaer, J. Als-Nielsen, M. Lahav, L. Leiserowitz, Two-dimensional crystallography of amphiphilic molecules at the air–water interface, Angew. Chem. Int. Ed. Engl. 31 (1992) 130–152.
[25] M.C. Wiener, R.M. Suter, J.F. Nagle, Structure of the fully hydrated gel phase of dipalmitoylphosphatidylcholine, Biophys. J. 55 (1989) 315–325.
[26] P.E. Harper, D.A. Mannock, R.N. Lewis, R.N. McElhaney, S.M. Gruner, X-ray diffraction structures of some phosphatidylethanolamine lamellar and inverted hexagonal phases, Biophys. J. 81 (2001) 2693–2706.
[27] M. Hereć, A. Islamov, A. Kuklin, M. Gagoś, W.I. Gruszecki, Effect of antibiotic amphotericin B on structural and dynamic properties of lipid membranes formed with egg yolk phosphatidylcholine, Chem. Phys. Lipids 147 (2007) 78–86.

[28] H.W. Meyer, K. Semmler, W. Rettig, W. Pohle, A.S. Ulrich, S. Grage, C. Selle, P.J. Quinn, Hydration of DMPC and DPPC at 4 degrees C produces a novel subgel phase with convex–concave bilayer curvatures, Chem. Phys. Lipids 105 (2000) 149–166.
[29] Z.V. Leonenko, E. Finot, H. Ma, T.E. Dahms, D.T. Cramb, Investigation of temperature-induced phase transitions in DOPC and DPPC phospholipid bilayers using temperature-controlled scanning force microscopy, Biophys. J. 86 (2004) 3783–3793.
[30] C. Hofsass, E. Lindahl, O. Edholm, Molecular dynamics simulations of phospholipid bilayers with cholesterol, Biophys. J. 84 (2003) 2192–2206.
[31] T. Kaasgaard, C. Leidy, J.H. Crowe, O.G. Mouritsen, K. Jorgensen, Temperature-controlled structure and kinetics of ripple phases in one- and two-component supported lipid bilayers, Biophys. J. 85 (2003) 350–360.
[32] A.H. de Vries, V. Knecht, S. Yefimov, A.E. Mark, S.I. Marrink, Simulations of phase transformations of lipid–water mixtures by molecular dynamics, Abstr. Pap. Am. Chem. Soc. 230 (2005) U1241–U.